Fermi National Accelerator Laboratory

FERMILAB-CONF-91/157-T

Observing the Higgs Boson and the ZZ lineshape

E. W. N. Glover*
Fermi National Accelerator Laboratory,
P. O. Box 500, Batavia, IL 60510, U.S.A.

May 31, 1991

Abstract

The discovery potential of the LHC and SSC for observing the Higgs boson in the 'gold plated' $pp \to ZZ \to \ell^+\ell^-\ell'^+\ell'^-$ mode is reviewed. The processes contributing to the ZZ lineshape are discussed and approximations to the Higgs boson signal compared with more precise calculations. Finally, the approximations to the Higgs boson signal available in parton shower Monte Carlos are summarized.

*SSC Fellow: Talk presented at the 25th Rencontres de Moriond, March 17th-25th 1991: Address after 1 September 1991, Physics Department, University of Durham, Durham DH1 3LE, England

Operated by Universities Research Association Inc. under contract with the United States Department of Energy

1 Introduction

One of the major objectives of the LHC and SSC is to search for the standard model Higgs boson in the mass range,

$$2M_Z \leq m_H \leq \mathcal{O}(1\ TeV), \tag{1.1}$$

where the dominant decay modes are $H \rightarrow W^+W^-$ and $H \rightarrow ZZ$. The cleanest or 'gold plated' mode for discovery is $H \rightarrow ZZ \rightarrow \ell^+\ell^-\ell'^+\ell'^-$ where $\ell = e,\ \mu$ and all four charged leptons are detected. In this case, each unlike sign lepton pair reconstructs the parent Z while the Higgs boson would appear as a resonance in the ZZ invariant mass distribution.

Fig. 1 shows the expected event rates in this channel for $m_H = 600$, 800 and 1000 GeV assuming an integrated luminosity of 10^4 pb^{-1} at both the LHC and SSC which corresponds to one 'year' of operation at the nominal luminosity of 10^{33} cm^{-2}s^{-1} [1]. The solid line represents the continuum background while the 'data' points are the signal with statistical errors. In order to simulate the leptonic coverage of future hadron collider experiments, a rapidity cut is imposed on the Z bosons,

$$|y_Z| < 2.5, \tag{1.2}$$

while to enhance the signal relative to the background, the Z boson is required to have a transverse momentum,

$$p_{TZ} > m_{ZZ}/4. \tag{1.3}$$

Furthermore the top quark mass m_t is assumed to be 120 GeV and the lepton identification efficiency to be 100%. With these assumptions and integrated luminosity, Fig. 1 shows that the LHC may be able to discover a 600 GeV Higgs as a resonance in the four lepton mode. However, too few events are produced in the resonance region to make a 800 GeV Higgs visible at the LHC. At the SSC, the cross sections are somewhat larger due to the higher beam energy and a 800 GeV Higgs is visible with about the same significance as a 600 GeV Higgs at the LHC. On the other hand, if we allow a factor 10 increase in integrated luminosity, the LHC can make up for the smaller beam energy and extend its discovery range up to 800 GeV. Recent studies making somewhat different assumptions for m_t, lepton coverage and the lepton identification efficiency [3, 4] reach similar conclusions for the discovery potential of the two machines.

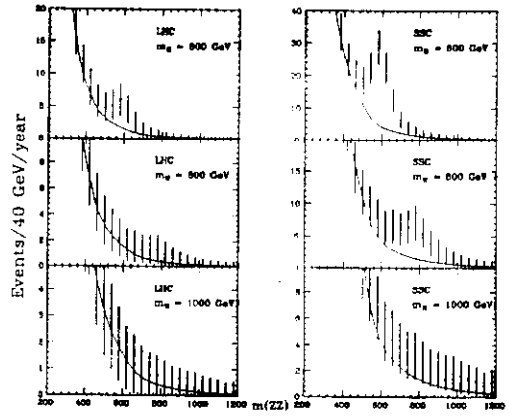

Fig. 1. Expected event rates for $pp \rightarrow ZZ \rightarrow \ell^+\ell^-\ell'^+\ell'^-$ as a function of m_{ZZ} at (a) the LHC and (b) the SSC. 'Data' points show the Higgs boson signal in 40 GeV bins for $m_H = 600$, 800 and 1000 TeV with statistical errors, while the continuous curve represents the background.

If $m_H > 800$ GeV, Fig. 1 shows that the signal is spread out over such a large range* that there is essentially no resonance structure, although there is an excess of events at large m_{ZZ}. In this case, by making a cut on the Z boson invariant mass $m_{ZZ} > m_{min}$, one can enhance the total number of signal events above m_{min} relative to the background [2, 1] which, for $m_H = 1$ TeV and 10^4 pb^{-1},

*It is worth noting that a 1 TeV Higgs has a width of about 500 GeV.

produces a 1.1 (4.4)σ deviation from the background with $m_{min} = 700$ GeV at the LHC (SSC) [1]. Such an analysis is extremely sensitive to our knowledge of the background, however we can clearly see that, *given the same integrated luminosity, the SSC is more sensitive to the presence of very heavy Higgs bosons or a strongly interacting electroweak sector than the LHC.*

2 The ZZ lineshape

The largest source of Z boson pairs is quark-antiquark annihilation [6],

$$q\bar{q} \to ZZ, \tag{2.1}$$

which contributes solely to the continuum background. Recently the next-to-leading QCD corrections to this process have been computed [7, 8], which show that the shape of the ZZ invariant mass distribution is significantly changed at large m_{ZZ} due to terms that grow as $\log^2(m_{ZZ}/M_Z)$. This indicates that higher order effects are important and that more theoretical work is needed to determine the $q\bar{q}$ contribution to the m_{ZZ} distribution at the 10% level.

There are two important mechanisms which contribute to the Higgs signal; the $\mathcal{O}(\alpha_s^2\alpha^2)$ 'gluon fusion' process [9, 11, 12],

$$gg \to H \to ZZ, \tag{2.2}$$

and the $\mathcal{O}(\alpha^4)$ 'vector boson fusion' process [10, 13, 14],

$$qq \to qqH \to ZZ. \tag{2.3}$$

In the gluon fusion process, the gluons couple to the Higgs boson via a top quark loop, so that this process is extremely dependent on m_t. In contrast, the vector boson fusion process depends only on the coupling of the Higgs with the W and Z and directly probes the electroweak symmetry breaking sector; the incoming quarks radiate vector bosons which then annihilate into a Higgs boson.

The contributions to the ZZ invariant mass distribution from these three processes is shown in Fig. 2 for $m_H = 800$ GeV at the SSC. The $q\bar{q}$ process is shown at leading order [6] and, apart from the $m_{ZZ} \sim 2M_Z$ threshold region, monotonically decreases with increasing m_{ZZ}. On the other hand, both the gluon fusion and vector boson fusion processes show a resonance structure around $m_{ZZ} \sim m_H$. On the low side of the resonance, the non-resonant gluon fusion graphs in which the Z bosons couple directly to the quark loop generate a significant cross section that falls sharply with increasing m_{ZZ}. It is also worth noting that, apart from the resonance region, the gluon fusion process becomes relatively less important at larger m_{ZZ} compared to the $q\bar{q}$ process. This is mainly due to the decrease in the gluon-gluon luminosity compared to that for $q\bar{q}$. In contrast, the vector boson fusion process is much flatter due to the exchange of massive vector bosons which generate logarithms of m_{ZZ}/M_Z and hence a harder m_{ZZ} spectrum.

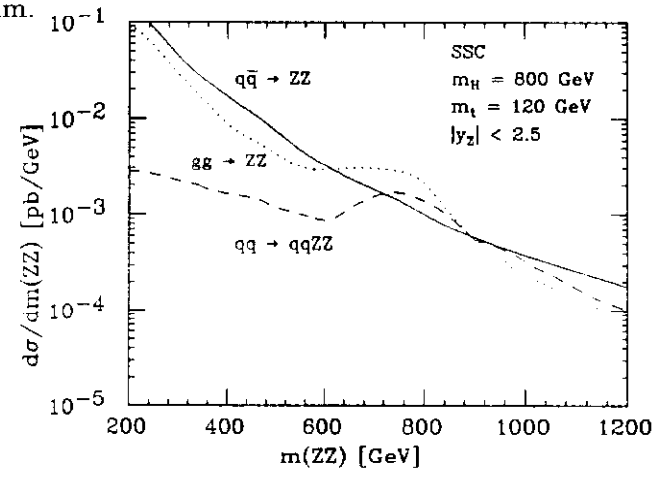

Fig. 2. The ZZ invariant mass distribution for $m_H = 800$ GeV at the SSC.

In the following, I will compare different matrix elements for the Higgs signal for the benchmark case $m_H = 800$ GeV with the following standard model parameters, $m_t = 120$ GeV, $M_Z = 91.1$ GeV, $\alpha = \alpha(M_Z) = 1/128$, $\sin^2\theta_W = 0.23$ and $M_W = M_Z \cos\theta_W = 80$ GeV. With these parameters, the width of an 800 GeV Higgs boson is $\Gamma_H = 258.8$ GeV. Furthermore, I will use the parton distributions of Duke and Owens (set 1) [5] evaluated at scale $Q^2 = \hat{s}/4$. Since all approximations are evaluated with the same input, our comparisons are independent of the choice of scales, *etc.*

3 The s-channel approximation

In the s-channel approximation [9, 10], only Higgs exchange graphs are included. The motivation for this is quite straightforward because in the resonance region $\sqrt{s} = m_{ZZ} \sim m_H$, the Higgs propagator has the form,

$$\frac{1}{s - m_H^2 + i m_H \Gamma_H} \sim \mathcal{O}\left(\frac{1}{\alpha}\right), \tag{3.1}$$

since $m_H\Gamma_H$ is $\mathcal{O}(\alpha)$ and the s-channel Higgs graphs are effectively lower order in the coupling. In this region it is therefore consistent at lowest order to include only Higgs exchange graphs in evaluating the cross section [9, 10]. This is completely analogous to including only the Z exchange graph at LEP energies. On the other hand, since the Higgs boson is relatively much wider than the Z, interference effects between the Higgs exchange and non-resonant graphs can be important even within the resonance region, particularly for the gluon fusion process where the gluon luminosity is sharply falling. This is shown in Fig. 3 for gluon fusion where the s-channel approximation is compared with the result obtained by including all tree level graphs [11, 12].

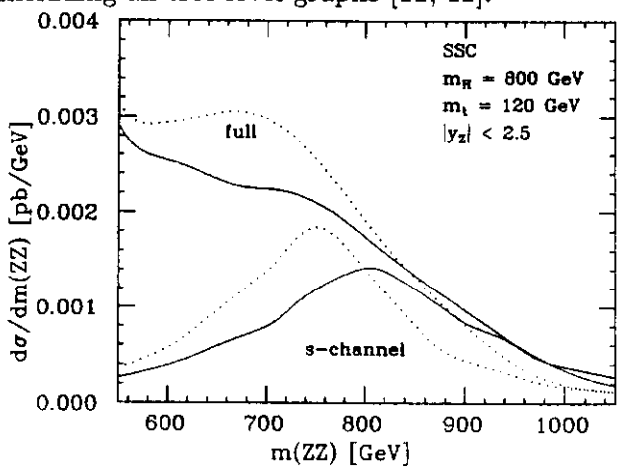

Fig. 3. The ZZ invariant mass distribution for $gg \to ZZ$ for $m_H = 800$ GeV at the SSC. The solid (dotted) lines show the full and s-channel approximation with a fixed (energy dependent) width.

It is important to remember that outside the resonance region at $m_{ZZ} >> m_H$, this approximation violates unitarity. Of course, here the Higgs graph is of the same order in coupling constant as all of the non-Higgs graphs [11, 12, 13, 14]. When all graphs are included unitarity is preserved outside the resonance region. *The s-channel approximation should only be used within the resonance region.*

4 The Higgs propagator

The bare Higgs propagator is given by, $1/(s - m_0^2)$, where m_0 is the bare Higgs mass. When $s - m_0^2 \sim \mathcal{O}(\alpha)$, a certain class of higher order corrections, the set of one-particle-irreducible (1PI) self energy graphs, may be resummed to give the effective propagator,

$$\frac{1}{s - m_H^2 + \mathcal{I}m\ \Pi(s)}, \tag{4.1}$$

where $\Pi(s)$ is the 1PI self energy, and,

$$\mathcal{I}m\ \Pi(s) \sim \alpha\frac{s^2}{M_Z^2} + \mathcal{O}(\alpha^2) \sim \alpha\frac{m_H^4}{M_Z^2} + \mathcal{O}(\alpha^2). \tag{4.2}$$

Note that $\mathcal{I}m\ \Pi(m_H^2) = m_H\Gamma_H$. At lowest order, it is therefore consistent to use either a fixed width (as in the previous section) or an energy dependent width. On the other hand, the energy dependent width is in principle more correct since the self energy is a function of s and not m_H. The difference between the two is illustrated in Fig. 3. The s-dependent width shifts the resonance to smaller m_{ZZ} and significantly modifies the shape. This is easily understood since the effective width beneath $m_{ZZ} = m_H$ is reduced thus increasing the cross section while the opposite occurs above the resonance [15]. *At lowest order all four curves are equivalent*, although they differ at next-to-leading order. Current theoretical thought [15] suggests that including all tree level diagrams with an energy dependent width is the best thing to do, however, to determine a fully consistent cross section at next-to-leading order requires a significant theoretical input before the supercolliders commence operation.

It is important to note that outside the resonance region, it is inconsistent to resum these self energy graphs and the Higgs propagator should therefore be $1/(s - m_H^2)$. Using an energy dependent width at $s >> m_H^2$ suppresses the Higgs exchange graphs so that unitarity is not violated in the s-channel approximation but is violated in the full calculation. In both cases, this is not a correct thing to do.

5 The effective W approximation

In the effective W approximation, gauge boson distribution functions $f^q_{\lambda,V}(x)$ describe the probability that on-shell vector boson V with polarisation λ is found carrying fraction x of the parent quarks momentum [10, 16]. The vector boson process is thus reduced to the $2 \to 2$ processes $WW \to ZZ$ and $ZZ \to ZZ$ convoluted with the gauge boson distribution functions while the quarks scatter at very small angles. As with ordinary parton distributions, these gauge boson distributions are evaluated at a scale Q^2 which is a scale associated with the hard process, typically m_{ZZ}^2 or p_{TZ}^2. Unfortunately, the distributions for transversly polarised gauge bosons depend strongly on the scale choice and lead to an unreliable prediction as shown in Fig. 4. This is not the case for longitudinally polarised gauge bosons which are essentially scale independent and which, after all, couple strongest to the Higgs boson. For comparison, Fig. 4 also shows the result obtained by including all of the $\mathcal{O}(100)$ tree level diagrams [13, 14]. We see that in the resonance region the effective W approximation works extremely well *provided that only longitudinal polarisations are included.*

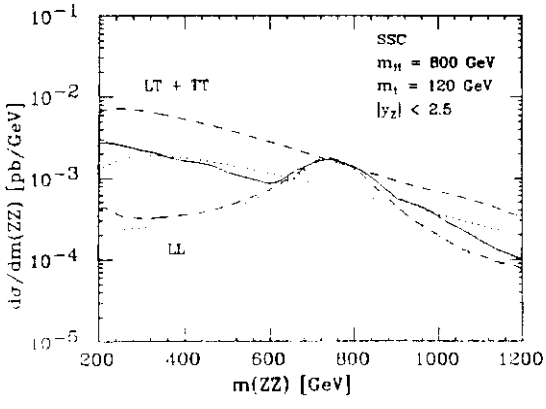

Fig. 4. The ZZ invariant mass distribution in the effective W approximation for $m_H = 800$ GeV at the SSC for $Q^2 = m_{ZZ}^2$ (dashed) and $Q^2 = m_{ZZ}^2/4$ (dotted) for longitudinal (LL) and transverse (LT+TT) polarisations. The exact $qq \to qqZZ$ calculation is shown solid.

6 The $m_H \to 0$ approximation

In this approximation, the full set of tree level diagrams is evaluated with m_H set to a small value which therefore satisfies unitarity everywhere [14]. In practice, the precise value of m_H does not matter provided $m_H << 2M_Z$. This is essentially equivalent to setting the partial waves involving the symmetry breaking sector to zero and represents the minimal contribution to the ZZ lineshape from both gluon fusion and vector boson fusion. Any strongly interacting Higgs sector or Higgs boson will increase the cross section above the $m_H \to 0$ limit. As illustrated by Fig. 5, this approximation shows that the ZZ background is increased by about 60% at the SSC relative to lowest order $q\bar{q} \to ZZ$ which is comparable to the effect of higher order QCD corrections. At the LHC this enhancement is about 30%. The background curve in Fig. 1 is thus obtained from the $q\bar{q} \to ZZ$ process added to the $m_H \to 0$ approximation for $gg \to ZZ$ and $qq \to qqZZ$.

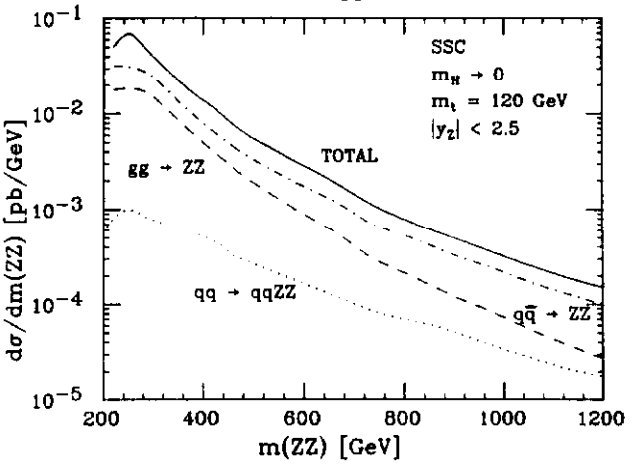

Fig. 5. The ZZ invariant mass distribution in the $m_H \to 0$ approximation at the SSC.

7 Shower Monte Carlos

By way of summary, Table 1 shows which approximations for ZZ production are available in PYTHIA [18], ISAJET [19] and HERWIG [20],

Table 1. ZZ production processes available in PYTHIA, ISAJET and HERWIG.

	PYTHIA	ISAJET	HERWIG
$q\bar{q} \to ZZ$	yes	yes	no
$Z \to f\bar{f}$	yes	yes	no
Γ_Z	yes	no	no
$gg \to ZZ$	no	no	no
$gg \to H \to ZZ$	yes	yes	yes
$Z \to f\bar{f}$	yes	yes	yes
Γ_Z	yes	no	yes
$m\Gamma$	$\Pi(s)$	$m_H\Gamma_H$	$m_H\Gamma_H$

$qq \to qqZZ$	no	no	no
$qq \to qqH \to qqZZ$	yes	no	yes
$Z \to f\bar{f}$	yes	-	yes
Γ_Z	yes	-	yes
$m\Gamma$	$\Pi(s)$	-	$m_H\Gamma_H$
$VV \to ZZ$	yes	yes	no
V polarisations	L only	L only	-
Z polarisations	L only	L + T	-
$Z \to f\bar{f}$	yes	yes	-
Γ_Z	yes	no	-
$m\Gamma$	$m_H\Gamma_H$	$m_H\Gamma_H$	-

References

[1] U. Baur and E. W. N. Glover, Fermilab preprint FERMILAB-PUB-90/154-T.

[2] M. S. Chanowitz and M. K. Gaillard, Nucl. Phys. **B261** (1985) 379.

[3] D. Froidevaux, Large Hadron Collider Workshop, CERN report CERN 90-10, Vol II (1990) 444.

[4] G. Trilling *et al.*, Letter of Intent by the SOLENOIDAL DETECTOR COLLABORATION, (1990).

[5] D. W. Duke and J. F. Owens, Phys. Rev. **D30** (1984) 49.

[6] R. W. Brown and K. O. Mikaelian, Phys. Rev. **D19** (1979) 922.

[7] B. Mele. P. Nason and G. Ridolfi, CERN preprint CERN-TH-5890 (1990).

[8] J. Ohnemus and J. F. Owens, Florida State preprint FSU-HEP-901212 (1990).

[9] H. Georgi, S. L. Glashow, M. E. Mahacek and D. V. Nanopoulos, Phys. Rev. Lett. **40** (1978) 692.

[10] R. N. Cahn and S. Dawson, Phys. Lett. **B136** (1984) 196, *ibid* **B138** (1984) 464(E).

[11] D. A. Dicus, C. Kao and W. W. Repko, Phys. Rev. **D36** (1987) 1570;
D. A. Dicus, Phys. Rev. **D38** (1988) 394.

[12] E. W. N. Glover and J. J. van der Bij, Nucl. Phys. **B321** (1989) 561.

[13] D. A. Dicus, S. L. Wilson and R. Vega, Phys. Lett. **B192** (1987) 231.

[14] U. Baur and E. W. N. Glover, Nucl. Phys. **B347** (1990) 12.

[15] S. S. D. Willenbrock and G. Valencia, Phys. Lett. **B247** (1990) 341.

[16] S. Dawson, Nucl. Phys. **B249** (1984) 42;
G. L. Kane, W. W. Repko and W. B. Rolnick, Phys. Lett. **B148** (1984) 367;
M. S. Chanowitz and M. K. Gaillard, Phys. Lett. **B142** (1984) 85.

[17] A. Abbasabadi and W. W. Repko, Phys. Rev. **D36** (1987) 289.

[18] H.-U. Bengtsson and T. Sjostrand, PYTHIA 5.4 (1990).

[19] F. Paige and S. Protopopescu, ISAJET 6.36 (1991).

[20] G. Marchesini, I. Knowles, M. Seymour and B. Webber, HERWIG 5.1 (1991).